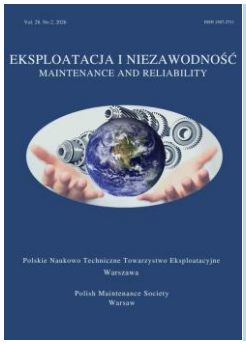

Eksploatacja i Niezawodnosc – Maintenance and Reliability
Volume 28 (2026), Issue 2
journal homepage: http://www.ein.org.pl

Article citation info:
He Y, Liu T, Wang H, Axle box bearing fault diagnosis via an adaptive feature mode decomposition based on dual-index fusion, Eksploatacja i Niezawodnosc – Maintenance and Reliability 2026: 28(2) http:/10.17531/ein/214468

Axle box bearing fault diagnosis via an adaptive feature mode decomposition based on dual-index fusion

Indexed by: Web of Science Group

Yong He[a,*], Tao Liu[a], Hong Wang[a]

[a] School Of Mechanical Engineering, Lanzhou Jiaotong University, China

Highlights

- A new fusion index is established to evaluate the sensitive mode component.
- The POFMD method is presented for axle box bearing early fault diagnosis.
- POFMD verify via different types of axle box bearings, beats VMD and Autogram.

Abstract

Considering that the early fault characteristics contained in the vibration signal of axle box bearings are easily affected by complex transmission paths and wheelset impact noise, a parameter optimization feature mode decomposition (POFMD) method based on dual-index fusion is proposed. Firstly, the square envelope of the time-domain signal autocorrelation function is introduced into the calculation of traditional Gini index and defined as ACSESGI. Secondly, the weight values of ACSESGI and the weight values of squared envelope kurtosis of different mode components obtained from FMD are calculated respectively. Finally, the above two weight values are added together and utilized as the objective function for parameter optimization. The effectiveness of presented method is verified through early fault diagnosis results of scaled-down axle box bearings and full-size axle box bearings, and its superiority was further validated by comparing with variational mode decomposition and Autogram.

Keywords
axle box bearings, feature mode decomposition, dual-index fusion; parameter optimization, early fault diagnosis.

1. Introduction

As a crucial part of the train's mechanical transmission system, the condition of the axle box bearings directly influences the safe operation of the train [1-2]. Therefore, methodologies for the early fault diagnosis of these bearings have garnered considerable research interest in recent years [3-4].

Under the complex influence of external factors such as vibration signal transmission path and wheel tread damage, how to distinguish the early damages of axle box bearings from background noise remains a technical challenge. Therefore, Liu et al. [5] distinguished the periodic impulse components caused by axle box bearings and wheel tread defects through adaptive correlation kurtosis. Zhang et al. [6] used a time-delay kurtosis to adaptively locate the optimal frequency band after empirical wavelet transform (EWT). Pan et al. [7] established a health criterion based on the fault frequency information, and employed it to diagnosis the compound fault of wheelset bearings. Cheng et al. [8] established a new index called impulse-norm and extended it to the maximization impulse-norm deconvolution method, but the generalized impulse number in this indicator needs to be pre-set based on the theoretical fault frequency. To reduce the dependence of axle box bearing diagnosis method on prior knowledge of fault frequency, Ding et al. [9] proposed an envelope spectral kurtosis index that considers bandwidth. But the effectiveness of this

(*) Corresponding author.
E-mail addresses: Y. He (ORCID: 0000-0002-0241-339X) hylzjt2014@139.com, T. Liu (ORCID: 0009-0006-4777-7900) lt241534@163.com
H. Wang (ORCID: 0000-0003-1435-7433) wh@mail.lzjtu.cn

indicator depends on the division of different frequency bands using EWT. Xu et al. [10] established a hybrid entropy based on the fuzzy and random characteristics of signals, and utilized it to diagnosis the early fault of axle box bearings. However, there are still two preset parameters, embedding dimension and similarity tolerance, which will affect the calculation results of the hybrid entropy. Furthermore, Gu et al. [11] established the envelope entropy based on entropy theory, which is a parameterless indicator that does not require the embedding dimension in the calculation process.

To effectively separate the fault information from background noise and other interference components, not only high-performance signal adaptive processing methods, but also effective evaluation indicator that can simultaneously evaluate the impulsiveness and periodicity of vibration signals are needed. Many famous signal adaptive processing methods have been developed, such as empirical mode decomposition (EMD) [12] and local men decomposition (LMD) [13] need not preset any parameters, but they are affected by endpoint effects and mode aliasing. Although variational mode decomposition (VMD) [14] has been proved to be better than EMD in finding the correct mode, it needs an evaluation index to optimize the mode number and penalty factor [15]. To reduce the reliance of VMD method's performance on preset parameters, Dibaj et al. [16] calculated the correlation coefficients between all modes and the original signal, and took the value of correlation coefficient multiplied by the kurtosis of modes as the objective function in the VMD parameter optimization process. Similarly, He et al. [17] used the value of correlation coefficient multiplied by the envelope energy spectral kurtosis of modes as the objective function, and Wu et al. [18] took the value of the envelop kurtosis multiplied by the envelop spectrum kurtosis as the objective function. In the above studies, the impulse component in the vibration signals is mainly measured by the improvement of the kurtosis index.

Enlightened by the above research methods for signal decomposition method, feature mode decomposition (FMD) was proposed [19]. FMD constructs finite impulse response (FIR) filter bank by maximizing the correlated kurtosis, and has stronger anti-interference ability against background noise. However, the mode number N and filter length L still need to be determined before the implementation of FMD, which reduces the parameter adaptability of FMD [20-21]. To overcome this problem, Chauhan et al. [22] employed the approximate entropy-to-kurtosis ratio as the criterion for optimizing FMD parameters. Although this fitness function can better evaluate the sparsity and impact of modes, the calculation of approximate entropy still relied on the two preset parameters of embedding dimension and similarity tolerance. Similarly, Yan et al. [23] proposed an indicator named SCKNR to identify the periodic impacts induced by bearing fault. However, the calculation of the feature energy ratio used in selecting sensitive mode still relies on advance knowledge related to fault frequencies.

In the view of above, this research presents POFMD based on dual-fusion index, for the incipient fault diagnosis of axle box bearings. The specific structure of this work is organized as follows. The Section 2 briefly introduces the FMD algorithm. The calculation process of dual-index fusion and POFMD method are explained in Section 3. The Section 4 introduces three fault experiments of axle box bearing, and the conclusion is outlined in Section 5.

2. Feature mode decomposition

FMD evenly divided the frequency bands of original signals into K segments by initializing FIR filter banks. The updating process of filter coefficients was defined as a constraint problem on constructing objective functions based on Correlated Kurtosis (CK). The specific steps can be expressed as [19]:

Step 1: Load the original signal x and preset parameters L, N and maximum iteration I ($i = 1,2,\cdots,I$).

Step 2: FIR filter banks is initialized through K Hanning Windows ($i = 1$).

Step 3: The filtered modes is obtained by iterating $u_k^i = x * f_k^i$, $*$ means the convolution operation, $k = 1,2,\cdots,K$.

Step 4: The filtering coefficients are updated, mode components u_k^i and estimated period T_k^i are obtained. The T_k^i is estimated by the time delay when the autocorrelation spectrum reaches the local maximum R_k^i after the zero crossing.

Step 5: Execute $i = i+1$, if the parameter i has not reached the maximum iteration I, return to Step 3. Otherwise, continue to perform Step 6.

Step 6: The correlation coefficient matrix $CC_{(K\times K)}$ of size $K\times K$ is constructed for every two modes, and the CK of these

modes is calculated in reference to T_k^i. The mode component exhibiting a higher CK value is preserved when comparing two similar modes, and K= K-1 is set.

Step 7: Determine whether K=N. If the criterion is not met, return to Step 3. Otherwise, the iteration is stopped and N mode components are obtained. The decomposed mode components can be denoted as y_n, and $n = 1,2,\cdots,N$.

3. Proposed approach

3.1. Dual-index fusion

Gini index (GI) is an effective sparsity index, which can better distinguish the background noise and repetitive transients [24]. To further enhance the ability of Gini index to identify the periodic impulses, the unbiased autocorrelation of the signal is first solved, and then the squared envelope spectrum of the unbiased autocorrelation is calculated. Finally, the squared envelope spectrum is arranged in ascending order and substituted into the Gini index formula for solving. This is because unbiased autocorrelation (AC) can not only effectively remove noise, random pulses, and other components unrelated to fault information in the signal, but also enhance the periodicity of the signal. Its specific calculation:

$$AC_{y_n}(\tau) = \frac{1}{M-|\tau|}\sum_{m=1}^{M-|\tau|} y_n(m) y_n(m+|\tau|) \tag{1}$$

Where M represents the length of mode y_n, $m = 1,2,\cdots,M$; τ represents the hysteresis coefficient, $\tau = -(M-1), -(M-2), \cdots, 0, \cdots (M-2), (M-1)$. The GI index based on AC square envelope spectrum is defined as ACSESGI, the ACSESGI of mode y_n is shown as follows:

$$ACSESGI_{y_n} = 1 - 2\sum_{z=1}^{Z} \frac{ACSES_{y_n,(z)}}{\|\mathrm{ACSES}_{y_n}\|_1}\left(\frac{Z-z+0.5}{Z}\right) \tag{2}$$

In the formula, ACSES represents the square envelope spectrum of mode y_n after unbiased autocorrelation solution, $ACSES_{y_n} = \left|FFT\left(\left|AC_{y_n}(\tau) + j \cdot Hilbert\left(AC_{y_n}(\tau)\right)\right|\right)\right|^2$. $Hilbert(\bullet)$ indicates the Hilbert transformation, $ACSES_{y_n,(z)}$ represents the amplitude of the z-th spectral line after the vector $ACSES_{y_n}$ is sorted in ascending order, Z represents the length of sequences after signal x is solved by unbiased autocorrelation, Z=2M-1. $\|\cdot\|_1$ is the L1 norm operation. Although ACSESGI can better evaluate the periodic components in vibration signals compared to traditional GI index, it has weaker resistance to background noise with strong periodicity such as harmonic wave. The squared envelope kurtosis (SEK) can further evaluate the impulse of periodic components [25]. The calculation process of SEK of mode component y_n is as follows:

$$SEK_{y_n} = \frac{\frac{1}{M}\sum_{m=0}^{M} {f_n}^4(m)}{\left(\frac{1}{M}\sum_{m=0}^{M-1} {f_n}^2(m)\right)^2} \tag{3}$$

Where,$f_n = (|y_n + j \cdot Hilbert(y_n)|)^2$. Due to ACSESGI being the same as the traditional Gini index, its calculation results are still between 0 and 1. Therefore, the SEK index was normalized to integrate the two indicators. The fusion index is defined as shown in Equation (4):

$$FI_{y_n} = ACSESGI_{y_n} + \frac{SEK_{y_n} - min(\mathrm{SEK})}{max(\mathrm{SEK}) - min(\mathrm{SEK})} \tag{4}$$

Where, $max(\bullet)$ and $min(\bullet)$ respectively represent the operation of taking the maximum and minimum values in the vector. The FI index can simultaneously evaluate the sparsity and impact of modes through the combination of SEK and ACSESGI. It not only avoids the insufficient sensitivity of traditional kurtosis index to periodic impulse, but also compensates for the insufficient sensitivity of ACSESGI index to early faults.

3.2. Parameter adaptive selected FMD

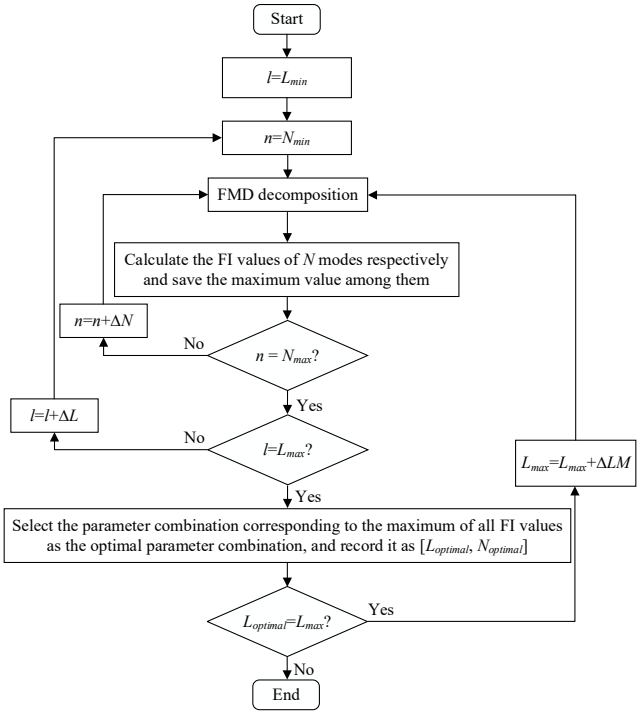

Fig. 1. FMD parameter optimization process.

Similar to the variational mode decomposition method, FMD also lacks the adaptability of parameters, that is, mode number N and filter length L need to predetermine. Therefore,

to overcome the above shortcoming, a POFMD method based on FI index and grid search method is proposed in this paper, and Fig. 1 demonstrates the adaptive parameter optimization process.

The procedure of POFMD method is shown as follows:

Step 1: Input the signal x and preset the parameter optimization range of N and L, $L \in [L_{min}, L_{max}]$, $N \in [N_{min}, N_{max}]$.

Step 2: Select L=L_{min} and N=N_{min}, and calculate the FI values of N modes obtained by decomposing the original signal x.

Step 3: Update $L = L + \Delta L$, $N = N + \Delta N$, and calculate the FI values of all modes under different parameter combinations by exhausting all combinations of L and N. The mode corresponding to the maximum FI value will be analyzed by envelope spectrum, and the parameter combination at this time will be taken as the best parameter combination, which is recorded as $N_{optimal}$ and $L_{optimal}$ respectively.

Step 4: If $L_{optimal}$ is equal to L_{max}, $L_{max} = L_{max} + \Delta LM$, and repeat Steps 2 and Step 3; otherwise, the optimization ends. The adaptive expansion of parameter optimization range not only avoids the excessive initial parameter optimization range leading to too long calculation time, but also avoids the maximum FI value being locally optimal.

4. Case studies

4.1. Case 1: A scaled–down axle box bearing

This section first uses a scaled‑down bogie axle box bearing test signal to further verify the effectiveness of POFMD method. The initial parameter optimization range is $L \in [10,100]$ ($\Delta L = 10, \Delta LM = 50$) and $N \in [2,8]$. The experimental devices are shown in Fig. 2. A machined defect was created on the bearing's inner race, and vibration signals were sampled at 20 kHz throughout the experiment. The axle box bearing rotation frequency of $f_r = 18.2$ Hz. According to the structural parameters displayed in Tab. 1, the inner race theoretical fault frequency $f_i = 152$Hz.

Table 1. The scaled-down axle box bearing parameters.

Parameters	Value
Inner diameter (mm)	30
Outside diameter (mm)	72
Rolling element diameter (mm)	10
Number of rolling elements	14
Rolling element contact angle (°)	11

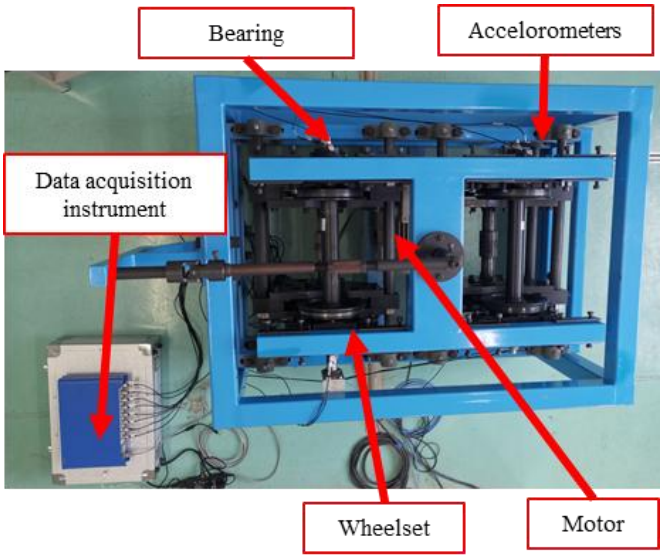

Fig. 2. The scaled‑down bogie test bench.

The low-frequency vibration generated by hunting motion will produce strong background noise, completely submerging the weak early fault feature signals, making it extremely difficult to extract these features. In Fig. 3, the time-domain waveform of the scaled-down axle box bearing exhibits heavily modulated continuous oscillation clusters due to severe background noise contamination, and no frequency components related to the inner race fault can be observed.

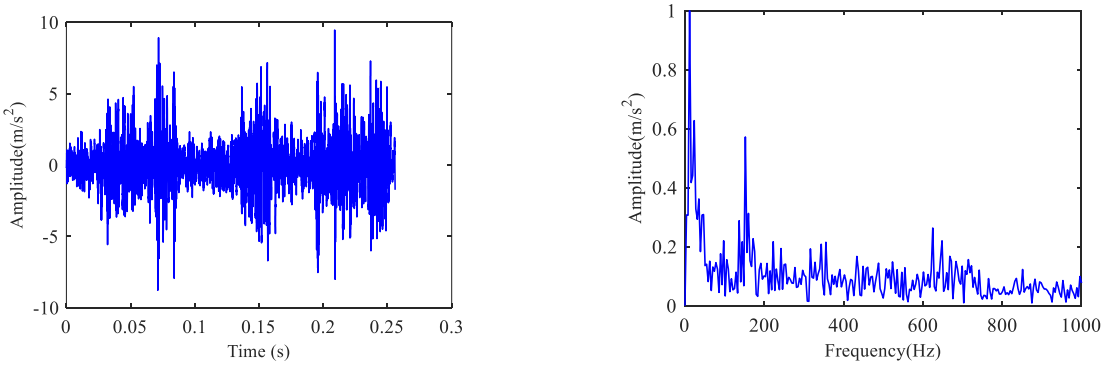

a) b)

Fig. 3. The scaled-down axle box bearing: (a) Waveform; (b) Envelope spectrum.

Furthermore, the parameter combination obtained using POFMD is a combination of N=8 and L=30. Among the eight mode components, mode component 7 has the highest FI value. From Fig. 4 (a), it can be seen that the strong background noise has been separated, and the highest spectral line in Fig. 4 (b) clearly shows the inner race fault. Concurrently, the 2nd harmonics (305Hz) are also clearly observed.

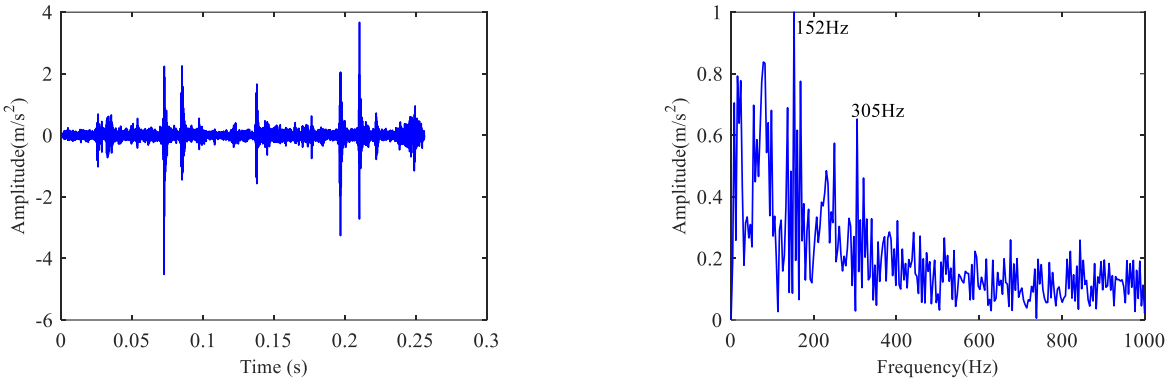

a) b)

Fig. 4. Mode component 7: (a) Waveform; (b) Envelope spectrum.

4.2. Case 2: A full-size axle box bearing

The passenger train axle box bearing experimental devices are shown in Fig. 5, the bearing model is 322880, and its structural parameters are displayed in Tab. 2. A spalling damage was created on the bearing's outer race, and sampling frequency was 40 000 Hz. The sensor type is HD 20100s, and the data acquisition instrument type is HD 2000. Based on its structural parameters and bearing rotation speed (330 rpm), the theoretical fault frequencies are $f_o = 32$Hz (outer race), $f_i = 45$Hz (inner race), and $f_b = 16$Hz (rolling element), respectively. Fig. 6 demonstrates that background noise and rotational frequency modulation cause the envelope spectrum peak is close to near the 2nd harmonics (86 Hz) of the inner race fault frequency. This may lead to the risk of misdiagnosis, namely that outer race damage might be misinterpreted as inner race fault. Furthermore, the parameter combination obtained using POFMD is a combination of N=2 and L=40. Among the two mode components, mode component 1 has the highest FI value. The fault frequency f_o and $2f_o$ (66Hz), $3f_o$ (94Hz) can be clearly observed from its envelope spectrum shown in Fig. 7.

Table 2. The passenger train axle box bearing parameters.

Parameters	Value
Inner diameter (mm)	130
Outside diameter (mm)	250
Rolling element diameter (mm)	32
Number of rolling elements	14
Rolling element contact angle (°)	0

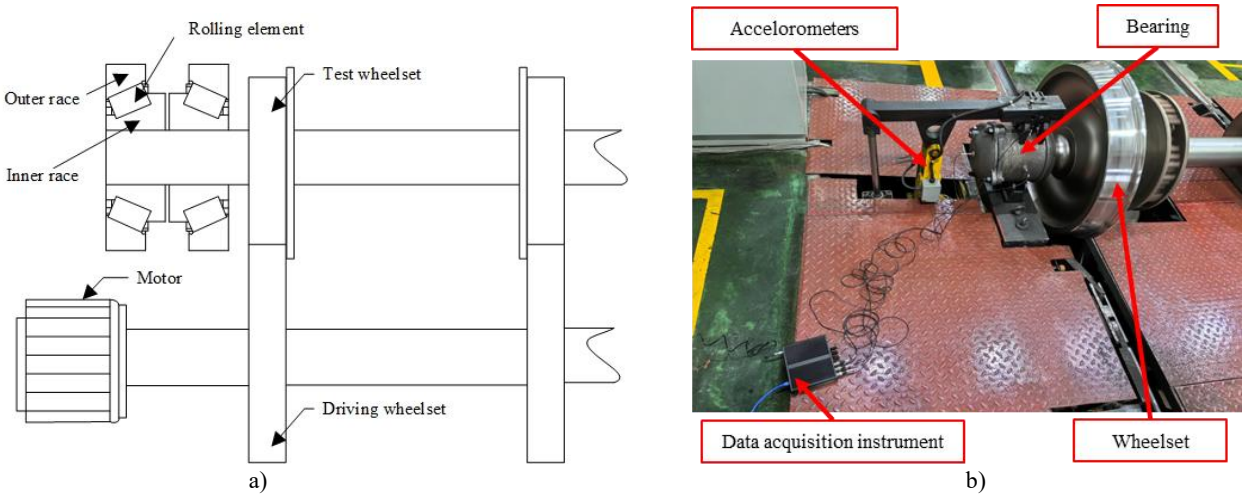

a) b)

Fig. 5. The passenger train axle box bearing experimental devices: (a) Structural diagram; (b) Composition of experimental devices.

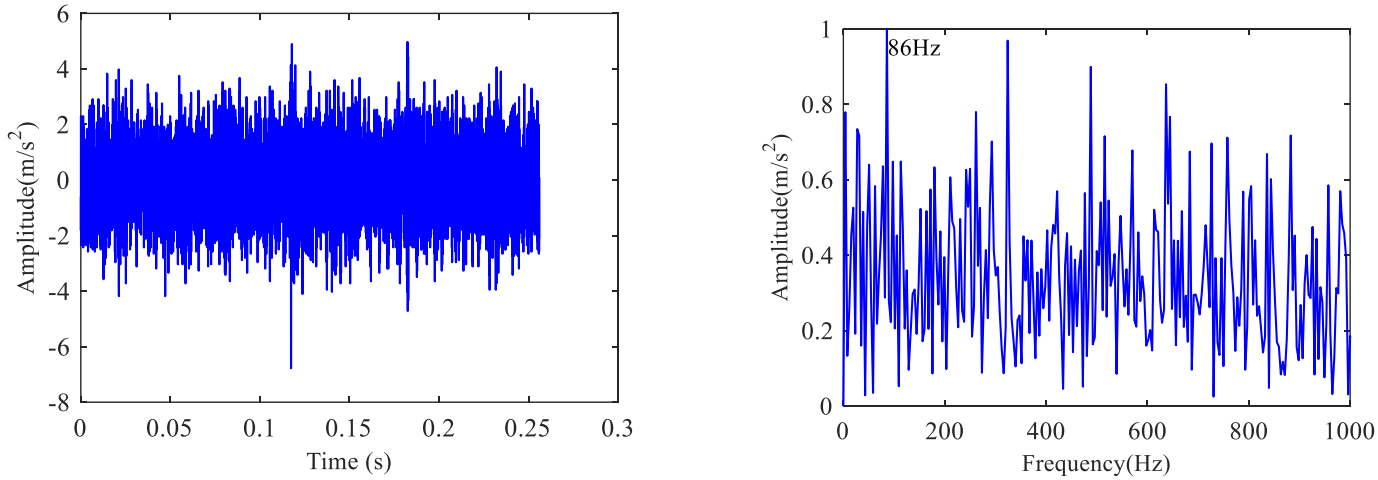

Fig. 6. The passenger train axle box bearing: (a) Waveform; (b) Envelope spectrum.

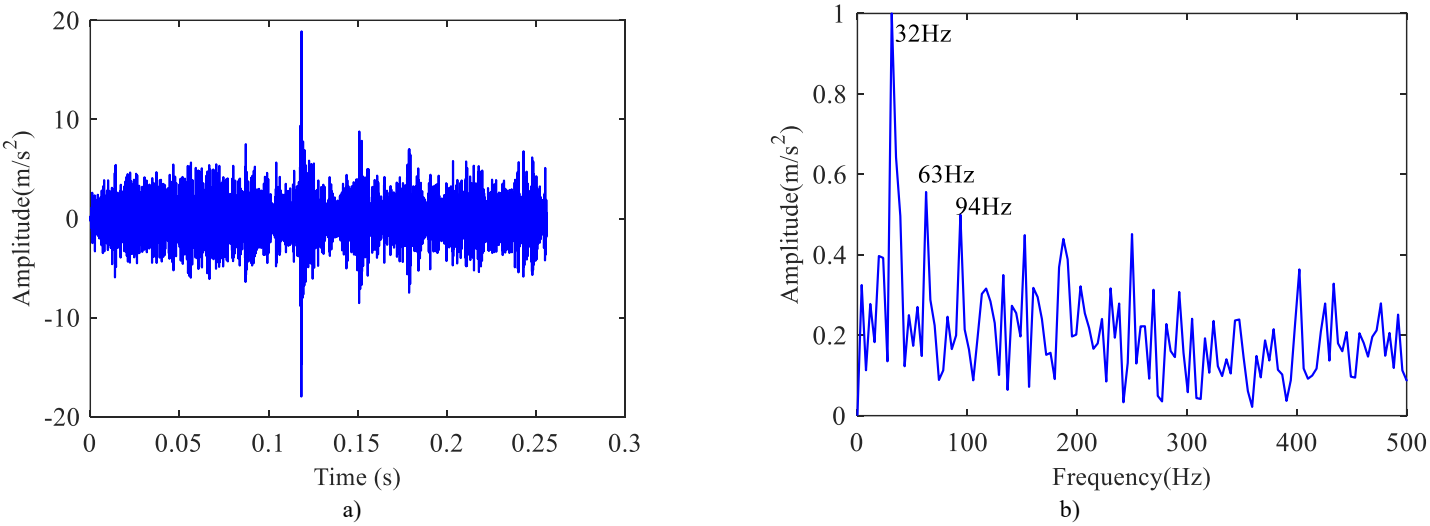

Fig. 7. Mode component 1: (a) Waveform; (b) Envelope spectrum.

The experimental devices for locomotive axle box bearing are composed of driving mechanism, data acquisition instrument, sensors, as shown in Fig. 8.

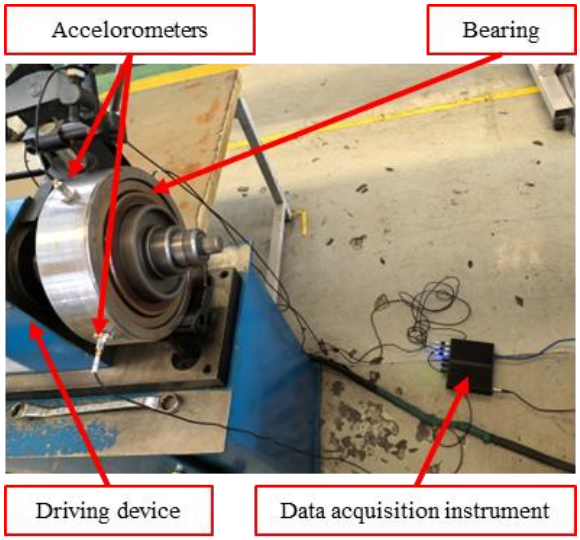

Fig.8. The locomotive train axle box bearing test bench.

During the experiment, the speed of the tested bearing was 500rpm (rotational frequency f_r=8.3 Hz), and the signal sampling frequency was 20 kHz. The fault type of the bearing is rolling element damage. According to the structural parameters shown in Tab. 3, the theoretical fault frequency can be obtained as f_b=27 Hz.

Fig. 9(a) demonstrates that the envelope spectrum peak of original signal is 160 Hz, and it is close to near $2f_i$ (the inner race fault frequency f_i=81 Hz). This makes a misdiagnosis risk where rolling element faults may be incorrectly identified as inner race faults. Furthermore, the parameter combination obtained using POFMD is a combination of N=8 and L=70. Fig. 9 (b) shows the envelope spectrum of mode 7 which is the optimal mode, and multiple harmonic information (i.e. f_b=27 Hz, $2f_b$=55 Hz, $3f_b$=78 Hz, $4f_b$=105 Hz) can be observed.

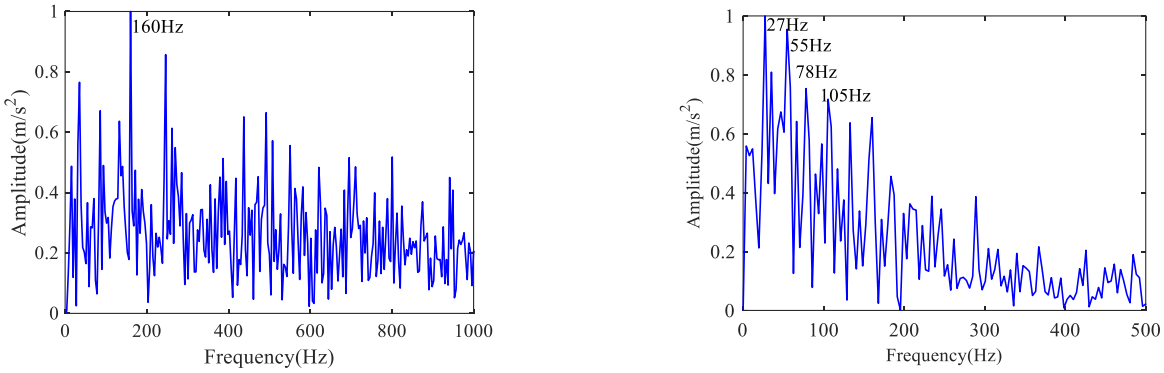

a) b)

Fig. 9. Envelope spectrum: (a) Original signal; (b) Mode 7.

4.3. Performance Comparison

In this section, the parameters of VMD are optimized with FI as the objective function (namely FI-VMD). The penalty factor in the initial parameter optimization range is $\alpha \in [100,1000]$ ($\Delta\alpha = 100$) and the number of modes is $K \in [2,8]$. Three set of axle box bearings is analyzed by VMD firstly, the VMD parameter optimization results of the scaled-down axle box bearing are α=100 and K=4. The envelope spectrum of mode 3 which is equivalent to the maximum FI is shown in Fig. 10, the second harmonic has not been demodulated from the background noise interference. Secondly, the VMD parameter optimization results of the passenger train axle box bearing are α=500 and K=8. The envelope spectrum of mode 2 which is equivalent to the maximum FI is shown in Fig. 11, compared to the diagnostic results in Fig. 7(b), POFMD can observe more harmonic information (i.e., the 3rd harmonic of the outer race fault frequency). Finally, the optimal parameter combinations of locomotive axle box bearing are α=100 and K=6. The envelope spectrum of mode 5, presented in Fig. 12, does not reveal any information indicative of a rolling element fault.

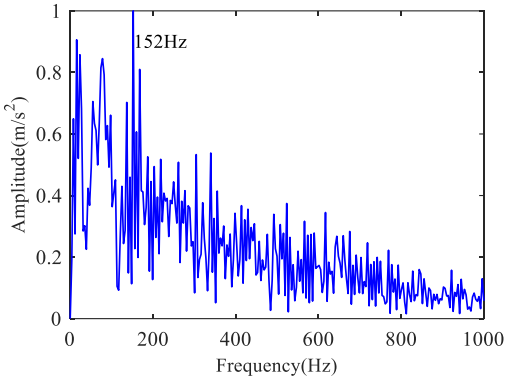

Fig. 10. Results of the scale-down axle box bearings based on FI-VMD

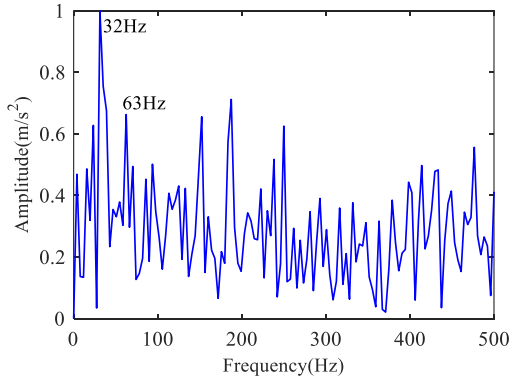

Fig. 11. Results of the passenger train axle box bearings based on FI-VMD

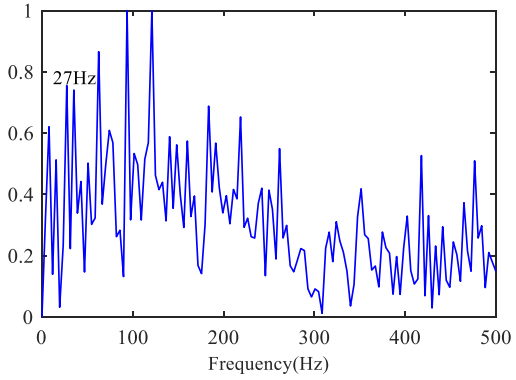

Fig. 12. Results of the locomotive axle box bearings based on FI-VMD.

Furthermore, considering that the autocorrelation kurtosis has good recognition characteristics for periodic impulses, the vibration of three set of axle box bearings is analyzed by the Autogram method [26]. Fig. 13 demonstrates that the fault type of the scaled-down axle box bearing is difficult to be effectively diagnosed in the envelope spectrum of the optimal Node 2.3 (that is, the third node on the second level) under the interference of other spectral lines. Meanwhile, the frequency doubling information of the passenger train axle box bearing in Fig. 14(b) is not as rich as the POFMD method, and the locomotive axle box bearing fault feature cannot be identified in Fig. 15. According to the above comparison results, the POFMD based on the FI has better advantages in the early fault diagnosis.

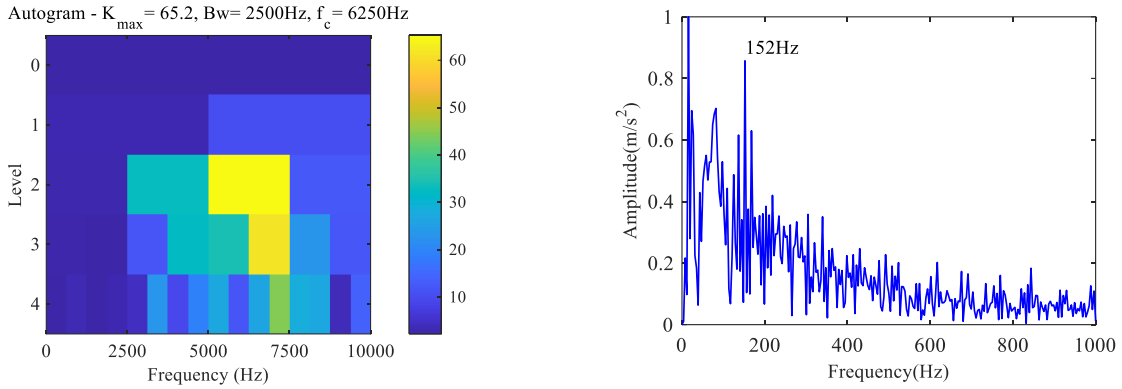

a) b)

Fig. 13. Results of the scaled-down axle box bearing: (a) Autogram; (b) Node 2.3 envelope spectrum.

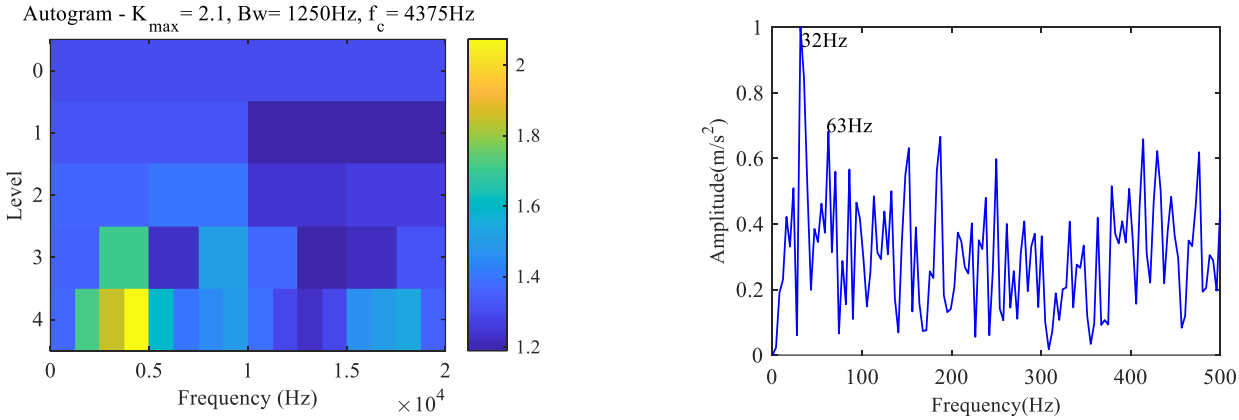

a) b)

Fig. 14. Results of the passenger train axle box bearing: (a) Autogram; (b) Node 4.4 envelope spectrum.

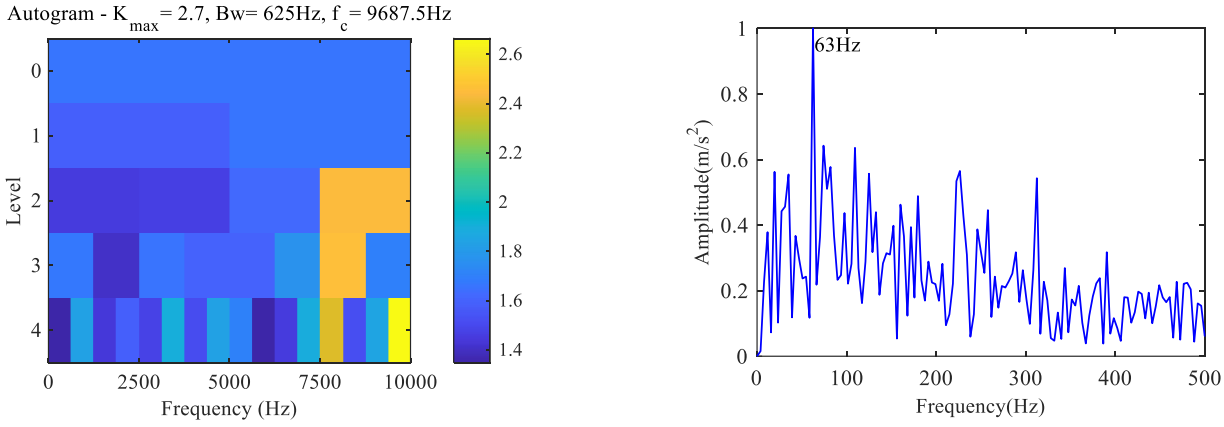

a) b)

Fig. 15. Results of the locomotive axle box bearing: (a) Autogram; (b) Node 4.16 envelope spectrum.

5. Conclusion

(1) Unlike existing research methods for optimizing FMD parameters, the proposed POFMD method based on the novel fusion index that combines ACSESGI and SEK, whose calculation process does not rely on prior knowledge or preset parameters. Therefore, the POFMD method has stronger adaptability and is more convenient for application in the engineering diagnosis of train axle box bearings.

(2) The diagnostic results of scaled-down axle box bearings and full-size axle box bearings show that the fusion index has good sensitivity to both periodic and impulsive components in vibration signals, and can effectively detect early faults from the complex background noise of axle box bearings. By comparing with the diagnostic results of VMD and Autogram, the superiority of the presented method is confirmed.

Acknowledgements

This study is sponsored by the National Natural Science Foundation of China (No. 72561016) and the Innovation Fund Project of Lanzhou Jiaotong University and Tianjin University (No. LH2024006).

References

1. Chen B Y, Zhang W H, Song D L, et al. Squared Envelope Sparsification Via Blind Deconvolution and Its Application to Railway Axle Bearing Diagnostics[J]. Structural Health Monitoring, 2023, 22(6): 3637-3658. https://doi.org/10.1177/14759217231151585.
2. Chen S Q, Guo L, Fan J J, et al. Bandwidth-Aware Adaptive Chirp Mode Decomposition for Railway Bearing Fault Diagnosis[J]. Structural Health Monitoring, 2024, 23(2):876-902. DOI: 10.1177/14759217231174699.
3. Zhang K, Yang G S, Yang M R, et al. LSESgram: A Novel Approach for Optimal Demodulation Band Selection in Rolling Bearing Fault Diagnosis[J]. Eksploatacja i Niezawodność – Maintenance and Reliability, 2026, 28(1): 208154. DOI:10.17531/ein/208154.
4. Li J X, Liu Z W, Qiu M, et al. Fault Diagnosis Model of Rolling Bearing Based on Parameter Adaptive VMD Algorithm and Sparrow Search Algorithm-Based PNN[J]. Eksploatacja i Niezawodność – Maintenance and Reliability, 2023, 25(2): 163547. DOI:10.17531/ein/163547.
5. Liu Z C, Yang S P, Liu Y Q, et al. Adaptive Correlated Kurtogram and Its Applications in Wheelset-Bearing System Fault Diagnosis[J]. Mechanical Systems and Signal Processing, 2021, 154:107511.DOI:10.1016/j.ymssp.2020.107511.
6. Zhang Q S, Ding J M, Zhao W T. An Adaptive Boundary Determination Method for Empirical Wavelet Transform and Its Application in Wheelset-Bearing Fault Detection in High-Speed Trains[J]. Measurement, 2021, 171:108746.DOI:10.1016/j.measurement.2020.108746.
7. Pan Y L, Yi C, Song X W, et al. A Novel Adaptive Resonant Band Detection Method Based on Cyclostationarity for Wheelset-Bearing Compound Fault Diagnosis[J]. Measurement, 2023, 213:112770.DOI:10.1016/j.measurement.2023.112770.
8. Cheng Y, Chen B Y, Mei G M, et al. A Novel Blind Deconvolution Method and Its Application to Fault Identification[J]. Journal of Sound and Vibration, 2019, 460:114900. DOI:10.1016/j.jsv.2019.114900.
9. Ding J M, Ding C C.Automatic Detection of a Wheelset Bearing Fault Using a Multi-Level Empirical Wavelet Transform[J]. Measurement, 2019, 134:179-192. DOI:10.1016/j.measurement.2018.10.064.
10. Xu C J, Yang J T, Zhang T Y, et al. Adaptive Parameter Selection Variational Mode Decomposition Based on a Novel Hybrid Entropy and Its Applications in Locomotive Bearing Diagnosis[J]. Measurement, 2023, 217:113110. DOI:10.1016/j.measurement.2023.113110.
11. Gu R, Chen J, Hong R J, et al. Incipient Fault Diagnosis of Rolling Bearings Based on Adaptive Variational Mode Decomposition and Teager Energy Operator[J]. Measurement, 2020, 149:106941. DOI:10.1016/j.measurement.2019.106941.
12. Ye X R, Hu Y F, Shen J X, et al. An Adaptive Optimized TVF-EMD Based on a Sparsity-Impact Measure Index for Bearing Incipient Fault Diagnosis[J]. IEEE Transactions on Instrumentation and Measurement, 2021, 70:1-11.DOI:10.1109/TIM.2020.3044517.
13. Li X, Ma J, Wang X D, et al. An Improved Local Mean Decomposition Method Based on Improved Composite Interpolation Envelope and Its Application in Bearing Fault Feature Extraction[J]. ISA Transactions, 2020, 97:365-383.DOI:10.1016/j.isatra.2019.07.027.
14. Dragomiretskiy K, Zosso D. Variational Mode Decomposition[J].IEEE Transactions on Signal Processing, 2014, 62(3):531-544. DOI:10.1109/TSP.2013.2288675.
15. Liu S S, Zhao R, Yu K P, et al. Output-Only Modal Identification Based on the Variational Mode Decomposition (VMD) Framework[J]. Journal of Sound and Vibration, 2022, 522:116668. DOI:10.1016/j.jsv.2021.116668.

16. Dibaj A, Hassannejad R, Ettefagh M M, et al. Incipient Fault Diagnosis of Bearings Based on Parameter-Optimized VMD and Envelope Spectrum Weighted Kurtosis Index with a New Sensitivity Assessment Threshold[J].ISA Transactions, 2021, 114:413-433. DOI:10.1016/j.isatra.2020.12.041.
17. He X Z, Zhou X Q, Yu W N, et al. Adaptive Variational Mode Decomposition and Its Application to Multi-Fault Detection Using Mechanical Vibration Signals[J]. ISA Transactions, 2021, 111:360-375. DOI:10.1016/j.isatra.2020.10.060.
18. Wu Q B, Gao Q W, Lu Y X, et al. Incipient Fault Diagnosis Method Via Joint Adaptive Signal Decomposition[J].IEEE Sensors Journal, 2024, 3414299.DOI:10.1109/JSEN.2024.3414299.
19. Miao Y H, Zhang B Y, Li C H, et al. Feature Mode Decomposition: New Decomposition Theory for Rotating Machinery Fault Diagnosis[J]. IEEE Transactions on Industrial Electronics, 2023, 70(2):1949-1960.DOI:10.1109/TIE.2022.3156156.
20. Zuo J Y, Lin J, Miao Y H. Period Enhanced Feature Mode Decomposition and Its Application for Bearing Weak Fault Feature Extraction[J]. Measurement Science and Technology, 2024, 35:116127.DOI:10.1088/1361-6501/ad6b42.
21. Ruan X L, Yuan R, Zhang D, et al. Iterative Feature Mode Decomposition: A Novel Adaptive Denoising Method for Mechanical Fault Diagnosis[J]. Measurement Science and Technology, 2024, 35:096101. DOI:10.1088/1361-6501/ad4fb2.
22. Chauhan S, Vashishtha G, Kumar R, et al. An Adaptive Feature Mode Decomposition Based on a Novel Health Indicator for Bearing Fault Diagnosis[J]. Measurement, 2024, 226:114191. DOI:10.1016/j.measurement.2024.114191.
23. Yan X A, Jia M P. Bearing Fault Diagnosis Via a Parameter-Optimized Feature Mode Decomposition[J]. Measurement, 2022, 203:112016. DOI:10.1016/j.measurement.2022.112016.
24. Miao Y H, Wang J J, Zhang B Y, et al. Practical Framework of Gini Index in the Application of Machinery Fault Feature Extraction[J]. Mechanical Systems and Signal Processing, 2022, 165:108333. DOI:10.1016/j.ymssp.2021.108333.
25. Li Y J, Zhang F, Xiong Q, et al. A Secondary Selection-Based Orthogonal Matching Pursuit Method for Rolling Element Bearing Diagnosis[J]. Measurement, 2021, 176:109199.DOI:10.1016/j.measurement.2021.109199.
26. Moshrefzadeh A, Fasana A. The Autogram: An Effective Approach for Selecting the Optimal Demodulation Band in Rolling Element Bearings Diagnosis[J].Mechanical Systems and Signal Processing, 2018, 105:294-318. DOI:10.1016/j.ymssp.2017.12.009.